Check for updates

Rapid assembly of mixed thiols for toll-like receptor-based electrochemical pathogen sensing†

Rajesh G. Pillai, [ID] [a] Khalid Azyat,[a] Nora W. C. Chan[b] and Abebaw B. Jemere [ID] *[acd]

Herein, we describe a rapid and facile fabrication of electrochemical sensors utilizing two different toll-like receptor (TLR) proteins as biorecognition elements to detect bacterial pathogen associated molecular patterns (PAMPs). Using potential-assisted self-assembly, binary mixtures of 11-mercaptoundecanoic acid (MUA) and 6-mercapto-1-hexanol (MCH), or MUA and an in-house synthesized zwitterionic sulfobetaine thiol (DPS) were assembled on a gold working electrode within 5 minutes, which is >200 times shorter than other TLR sensors' preparation time. Electrochemical methods and X-ray photoelectron microscopy were used to characterize the SAM layers. SAMs composed of the betaine terminated thiol exhibited superior resistance to nonspecific interactions, and were used to develop the TLR sensors. Biosensors containing two individually immobilized TLRs (TLR4 and TLR9) were fabricated on separate MUA-DPS SAM modified Au electrodes (MUA-DPS/Au) and tested for their response towards their respective PAMPs. The changes to electron transfer resistance in EIS of the TLR4/MUA-DPS/Au sensor showed a detection limit of 4 ng mL^{-1} for *E. coli* 0157:H7 endotoxin (lipopolysaccharide, LPS) and a dynamic range of up to 1000 ng mL^{-1}. The TLR4-based sensor showed negligible response when tested with LPS spiked human plasma samples, showing no interference from the plasma matrix. The TLR9/MUA-DPS/Au sensor responded linearly up to 350 µg mL^{-1} bacterial DNA, with a detection limit of 7 µg mL^{-1}. The rapid assembly of the TLR sensors, excellent antifouling properties of the mixed SAM assembly, small size and ease of operation of EIS hold great promise for the development of a portable and automated broad-spectrum pathogen detection and classification tool.

1 Introduction

Pathogens present an unparalleled threat to human lives as they can be transmitted through air, water or food. Effective early detection is of utmost importance to curb and contain pandemic and epidemic outbreaks. Conventional means of pathogen detection, identification and monitoring based on colony and culture counting, plaque neutralization tests and polymerase chain reaction are time consuming, expensive and inadequate for rapid and onsite analysis,[1] which is key for early intervention and disease containment. Biosensors have received increasing attention as an alternative to these laboratory-based tests due to their rapid response time,

portability and low-cost instrumentation.[1,2] Typical biosensors that employ nucleic acids and proteins as target recognizing entities provide specific and sensitive pathogen detection. However, for their effective use a potential cause of infection must be suspected and they are not suitable for screening emerging threats where the pathogen is unknown. To alleviate these limitations and boost biosecurity efforts, broad-spectrum biosensors that are capable of detecting any member of a broad group of related organisms using nonspecific reagents are highly sought after.[3,4] In the literature, several approaches are presented for broad-spectrum detection and classification of pathogens, including chemical-based optical sensors for bacteria detection,[5,6] PCR-mass spectrometry assays,[7,8] and optical and electrochemical sensors using toll-like receptor proteins (TLRs)[9–19] and antimicrobial peptides as nonspecific recognition moieties.[20–22] In a recent report, our group demonstrated that TLR-based electrochemical impedimetric sensors combined with microfluidic sample manipulation have potential for the development of miniaturized and portable bacterial detection and classification platforms.[19]

Toll-like receptor (TLRs) proteins, which are produced by innate immune cells, recognize key conserved molecular signatures present in pathogen classes. For example, TLR4

[a] National Research Council Canada- Quantum and Nanotechnologies Research Center, 11421 Saskatchewan Drive, Edmonton T6G 2M9, AB, Canada. E-mail: abebaw.jemere@nrc-cnrc.gc.ca

[b] Defence Research and Development Canada – Suffield Research Centre, Medicine Hat T1A 8K6, AB, Canada

[c] Department of Chemistry, Queen's University, Kingston K7L 3N6, ON, Canada

[d] Department of Chemistry, University of Waterloo, Waterloo N2L 3G1, ON, Canada

† Electronic supplementary information (ESI) available. See DOI: https://doi.org/10.1039/d4ay00983e

recognizes lipopolysaccharides (LPS) found in Gram-negative bacteria, TLR5 identifies flagellin of flagellated bacteria and TLR9 shows affinity to unmethylated cytosine–phosphate–guanine (CpG) oligodeoxynucleotides (ODNs) in bacterial and viral DNAs.[23] This class specificity of TLRs makes them appealing for the development of broad-spectrum pathogen detection and classification devices.[9–19] The construction of these sensors, however, relies on passive incubation of clean electrode surfaces in alkanethiol or N-heterocyclic carbene (NHC) solutions to form the biomolecule linker self-assembled monolayer (SAM) surfaces, taking several hours (even days) to attain well-packed and compact self-assembled monolayer (SAM) structures, and often suffers from reproducibility problems.[24,25]

In this work, we employed a potential-assisted SAM formation strategy to deposit mixed thiol SAMs on Au electrodes for fast and reliable TLR-based electrochemical pathogen sensor fabrication, and minimize nonspecific adsorption. Potential-assisted self-assembly has been shown to considerably reduce the adsorption dynamics of thiols and thiolated aptamers from several hours to several minutes and improve the reproducibility of sensor fabrication.[26–30] Mixed thiol SAMs, formed by co-adsorption of binary thiols where one thiolate with a functional headgroup anchors the biorecognition element and the other, as dilutant, provide convenient routes to immobilize biorecognition entities onto gold electrodes for sensing applications.[31,32] Moreover, mixed thiol SAMs have also been shown to prevent denaturation of the biorecognition entity, minimize non-specific protein adsorption, and improve the bioactivity of the sensor in comparison with one developed using homogeneous SAMs.[31,32] However, such mixed thiol SAMs are rarely reported in electrochemical impedance spectroscopy (EIS)-based pathogen sensor development.[33] Here, mixed SAMs of 11-mercaptoundecanoic acid (MUA) with 6-mercapto-1-hexanol (MCH) or with an in-house synthesized sulfobetaine thiol, 3-((3-mercaptopropyl)dimethylammonio)propane-1-sulfonate (DPS), were formed by applying a constant DC potential, and the self-assembly is compared with that formed by a conventional passive incubation technique. Zwitterionic compounds, such as sulfobetaines, are attractive materials for preventing biosensor fouling due to their high resistance to protein non-specific adsorption from complex media, stability and biocompatibility.[34] By employing an optimized potential and thiol ratio, compact and reproducible mixed thiol SAMs with excellent antifouling properties were formed within 5 minutes as opposed to the many hours (days) required to fabricate the above cited TLR sensors[9–18] reducing the sensor fabrication time by >200-fold. Two different TLRs (TLR4 and TLR9) were individually immobilized as active components of the biosensor surfaces and tested against their respective pathogen-associated molecular patterns (PAMPs). The antifouling properties of the commonly used dilutant MCH are compared against those of the zwitterionic sulfobetaine (DPS), with DPS modified electrodes showing superior performance. EIS of a TLR4 sensor fabricated using an MUA-DPS SAM showed negligible matrix effect when tested with LPS spiked human plasma samples,

demonstrating its potential applicability in real biological fluids.

We also report the development of an electrochemical TLR9-based bacterial DNA (CpG ODN) sensor using an MUA-DPS SAM modified gold electrode, yielding a dynamic range that covers clinically relevant concentrations of bacterial DNA known to cause the induction of innate immune response.[35,36] It is reported that bacterial DNA activates TLR9 in a concentration dependent manner; for example, 10–100 μg mL^{-1} E. coli DNA is needed to activate TLR9 in humans while >30 μg mL^{-1} E. faecalis DNA is effective in activating the protein.[36] There exists only one prior report on the development of a TLR9 bacterial sensor, where the sensor fabrication took more than 60 h yielding a narrow dynamic range of 5–20 μg mL^{-1} CpG ODN.[17] The rapid assembly, excellent antifouling properties and selectivity of the sensors reported here along with their potential for multiplexing and integration with microfluidic devices hold promise for future development of onsite-assembled, field-deployable broad-spectrum pathogen detection and classification platforms for early warning and diagnosis of pathogen contamination in various samples.

2 Materials and methods

2.1 Materials and chemicals

11-Mercaptoundecanoic acid (MUA, 95%), 6-mercapto-1-hexanol (MCH, 97%), ACS reagent grade potassium ferrocyanide trihydrate ($K_4[Fe(CN)_6] \cdot 3H_2O$, ≥99.0%), ACS reagent grade potassium ferricyanide ($K_3[Fe(CN)]_6$, ≥99.0%), ACS reagent grade potassium nitrate (KNO_3, ≥99.0%), bovine serum albumin (BSA, >96%), phosphate buffered saline tablets (PBS), BioUltra grade 4-morpholineethanesulfonic acid hydrate (MES, 99.5%), purum grade 1-ethyl-3-(3-dimethylaminopropyl)-carbodiimide hydrochloride (EDC, ≥98%), N-hydroxysuccinimide (NHS, 98.0%), ACS reagent grade ethanolamine (≥99%), lipopolysaccharide (LPS, serotype 0127: B8), and endotoxin-free water were obtained from Sigma-Aldrich (Oakville, ON, Canada) and used as received. Anhydrous ethyl alcohol (USP grade) was purchased from Commercial Alcohols Inc. (Brampton, ON, Canada). Recombinant human toll-like receptor 4-myeloid differentiation-2 (rhTLR4-MD-2) complex (carrier-free) was purchased from R&D Systems (Minneapolis, MN, USA). (In vivo, MD-2 protein is required for TLR4-mediated responses to bacterial LPS; here the sensor fabricated with the TLR4-MD-2 complex is labeled as a TLR4 sensor for simplicity.) Human toll-like receptor 9 (TLR9) and cytosine–phosphate–guanine oligodeoxynucleotides, CpG ODN (ODN 2006, ODN 2006 FITC, ODN 2006 control), were purchased from Invivogen Inc. (San Diego, CA, USA). The negative control of ODN 2006 (ODN 2137) contains the GpC nucleotide, instead of CpGs, and does not induce TLR9 activity. All biomolecules were reconstituted according to manufacturer recommended protocols. Endotoxin-free water was used to prepare the respective TLR and PAMP solutions whereas deionized ultrapure water with a resistivity of 18.2 MΩ cm was used for preparing all other solutions. The sulfobetaine thiol 3-[(3-mercaptopropyl)dimethylammonio]propane-1-sulfonate ($C_8H_{19}NO_3S \cdot HCl$, DPS)
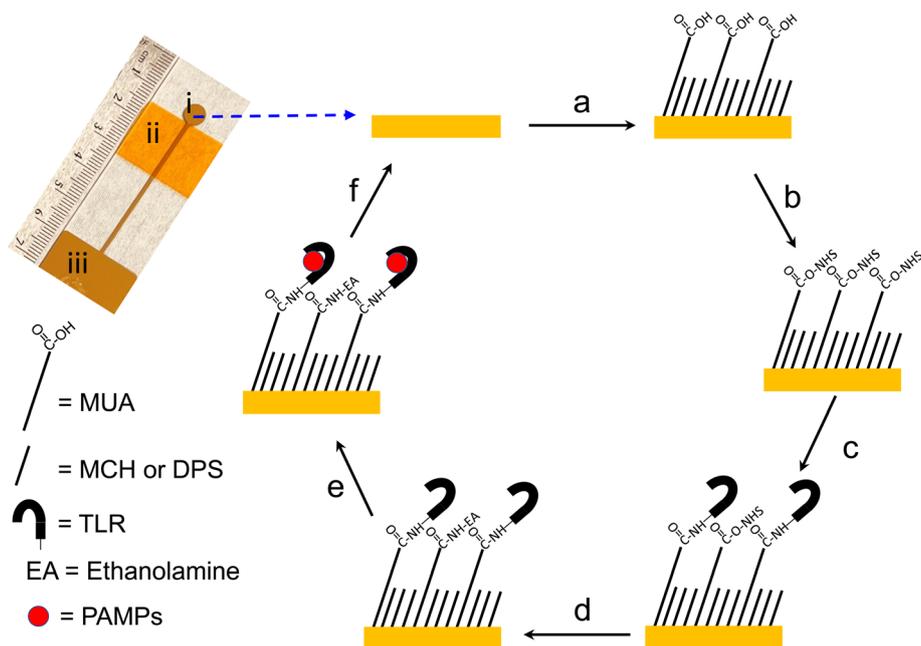
Scheme 1 Graphical representation of the fabrication of a reusable TLR biosensor on gold electrodes: (a) electrodeposition of mixed SAMs, (b) EDC/NHS activation, (c) TLR attachment, (d) deactivation by ethanolamine, (e) TLR sensor exposed to the target analyte (PAMPs), and (f) disassembling of the sensor and electrode cleaning. A photograph of the Au working electrode is also shown on the top left corner of the scheme; (i) is a circular WE with an area of 0.28 cm^2, (ii) a Kapton tape used to isolate the WE from the contact Au wire, and (iii) a gold contact pad.

was synthesized in-house following a published protocol for a similar compound[37] and characterized by ^{1}H NMR. Details of the synthesis steps and NMR characterization are given in ESI Scheme S1 and Fig S1.† ^{1}H NMR spectra were recorded with a Varian 600 MHz spectrometer. Chemical shifts are reported in parts per million (ppm, δ unit), while coupling constants are reported in Hertz (Hz).

Deionized (DI) water with a resistivity of 18 MΩ cm (Milli-Q UV Plus Ultra-Pure Millipore System) was used to prepare buffers (10 mM phosphate buffered saline, PBS, pH 7.4), 50 mM Tris buffer (pH 8.5) and 10 mM MES buffer (pH 5.5) as well as for rinsing electrodes. Note: Proper PPE (such as safety glasses, gloves and laboratory coats) must be worn during sample preparation, sensor fabrication and conducting experiments. Human plasma samples should be handled in an approved biosafety level facility. Platelet removed human plasma was obtained from the Research Division of the Canadian Blood Services and kept at −80 °C until being used. In accordance with the Canadian Blood Services policy, samples had been pooled to preserve donor anonymity and donors had provided consent. Ethical approval for the use of human blood was provided from the National Research Council Canada (reference number 2008-40) and the University of Alberta (reference number MS9_Pro0002363).

2.2 Electrode fabrication and TLR sensor preparation

Gold electrodes were fabricated at the University of Alberta NanoFab (Edmonton, AB) using a previously reported procedure.[38] Briefly, 100 nm gold and 15 nm titanium were sputtered on piranha (conc. $H_2SO_4 : H_2O_2$, 3 : 1 ratio) cleaned glass

microscope slides (Fisherfinest™ Premium, Fisher Scientific, Ottawa, ON, Canada) using an electron beam evaporator (Kurt J. Lesker Co., Clairton, PA) at a base pressure of 1×10^{-6} Torr and a metal shadow mask to define the working electrode (WE) area (0.28 cm^2). An optical image of the fabricated electrode is shown in Scheme 1.

The major fabrication steps followed in the preparation of the TLR biosensors are shown in Scheme 1. Au electrodes were first rinsed with ethanol, dried with Ar and electrochemically cleaned in 0.5 M H_2SO_4 by cycling between −0.2 V and +1.5 V (vs. Ag/AgCl) at 100 mV s^{-1} until the CV signal was stable (∼10 cycles). Electrodeposition of mixed SAMs on clean gold electrodes was then performed by applying +0.5 V vs. Ag/AgCl for 5 minutes using a 20 mL mixed thiol solution containing MUA-MCH or MUA-DPS (in a 1 : 3 ratio with a total thiol concentration of 10 mM) and 0.1 M LiClO$_4$ as the supporting electrolyte. Anhydrous ethanol was used as the solvent for MUA-MCH SAMs whereas a 50/50 (v/v%) ethanol/water mixture was used for MUA-DPS SAMs; a mixture of water and ethanol was used in the MUA-DPS self-assembly due to the low solubility of DPS in pure ethanol. After electrodeposition, the SAM modified electrodes were thoroughly washed with their respective solvents, gently dried with a stream of Ar and immersed in a solution of 50 mM EDC and 50 mM NHS, prepared in 100 mM MES buffer (pH 5.0) for 30 minutes to activate the carboxyl groups of MUA. The modified electrodes were then incubated with 200 μL of 5 μg mL^{-1} TLR4, prepared in 10 mM PBS (pH 7.4) or 2 μg mL^{-1} TLR9 prepared in 10 mM MES buffer (pH = 5.5) overnight at 4 °C to produce the two different sensor types. The two TLRs were prepared under different buffer conditions since these buffer

pHs were reported to be optimal for their interaction with their respective ligands. The interaction of TLR9 with bacterial DNA is reported to be optimal at slightly acidic pH (pH 5.5)[9,39] while the interaction of TLR4 with LPS is reported in pH 7.4 buffer.[11,13–19] The TLR modified sensors were then rinsed with either PBS or MES buffers and subsequently exposed to 1 M ethanolamine (prepared in 50 mM Tris buffer, pH 8.5) for 10 minutes to deactivate any unreacted NHS esters. The sensors were then washed with endotoxin-free water and dried with a gentle stream of Ar gas. Finally, the TLR sensors were tested for non-specific adsorption by incubating with 1 mg mL^{-1} BSA (in PBS buffer, pH 7.4) for 30 minutes. TLR biosensors with MUA-DPS mixed SAMs did not show any significant change in electrochemical impedance behavior (i.e. change transfer resistance, R_{CT}) after BSA exposure, and this mixed thiol composition was selected to fabricate the two TLR sensors. The sensors were incubated with an aliquot of 200 µL of their respective ligands for 30 minutes; LPS (prepared in 10 mM PBS buffer pH 7.4) for the TLR4 sensor and CpG ODN (prepared in 10 mM MES buffer pH 5.5) for the TLR9 sensor. The sensors were then thoroughly rinsed with their respective buffer solutions, and gently dried with a stream of Ar before electrochemical measurements.

The sensor fabrication steps were characterized by cyclic voltammetry (CV), EIS, X-ray photoelectron spectroscopy (XPS, AXIS 165 Spectrometer, Kratos Analytical Inc., Spring Valley, NY, USA) and fluorescence microscopy (Olympus IX81, Tokyo, Japan).

2.3 Electrochemistry

Electrochemical measurements. Electrochemical measurements were performed using a Gamry Reference 600™ potentiostat/galvanostat (Gamry Instruments Inc., Warminster, PA, USA). A three-electrode system consisting of a platinum coil counter electrode, a Ag/AgCl (3 M NaCl saturated with AgCl) reference electrode (BASi, West Lafayette, IN, USA) and a TLR modified gold working electrode were used in a 20 mL electrochemical cell. The redox couple was 1 mM K$_4$[Fe(CN)$_6$]/K$_3$[Fe(CN)$_6$] (1 : 1 ratio) prepared either in 0.1 M PBS (pH = 7.4) or in 0.1 M KNO$_3$, and was purged with Ar gas to remove dissolved oxygen prior to measurements. For CV experiments, the scan rate was 100 mV s^{-1}. EIS measurements were performed at open-circuit potential (vs. Ag/AgCl) over a frequency range of 0.1 Hz to 100 kHz with an AC pulse amplitude of 10 mV. The EIS data was fitted to a Randles equivalent circuit (shown as an inset in Fig. 2b) using a Gamry Echem Analyst software to obtain the value of circuit components. The difference in charge transfer resistance (R_{CT}) across the sensor's surfaces was used to construct calibration plots for LPS and CpG ODN. Flagellin (from *Salmonella typhimurium*) and ODN 2006 (containing GpC dinucleotide instead of CpG) were used as negative controls for the TLR4 and TLR9 sensors, respectively. Linear sweep voltammetry of the mixed thiol modified Au electrode was conducted using 0.1 M KNO$_3$ at a scan rate of 100 mV s^{-1}. Regeneration of the working Au electrode was achieved by electrochemical reductive desorption of the SAM layers using an

applied potential of −1.1 V vs. Ag/AgCl to the modified Au electrode for 3 min as described in our previous reports.[38,40]

2.4 Electrochemical quartz crystal microbalance

Electrochemical quartz-crystal microbalance (eQCM) measurements were performed using a Gamry EQCM 10M instrument with a polyetheretherketone (PEEK) static cell on 5 MHz gold-coated quartz crystals. Before SAM formation, the gold-coated QCM crystals were cleaned with freshly prepared piranha solution for a short time (30 s) followed by rinsing with copious amount of deionized water and drying in Ar. Electrochemical measurements were performed after getting a stable baseline for the QCM in 10 mM PBS buffer (pH 7.4). While continuously monitoring the QCM response, a 250 µL solution of TLR4 in PBS buffer was added to the cell to get a final solution concentration of TLR4 of 5 µg mL^{-1}.

2.5 Fluorescence microscopy

TLR9/MUA-DPS/Au sensors were exposed to fluorophore tagged CpG ODN (ODN-FITC), prepared in 10 mM MES buffer (pH = 5.5), for 1 hour. The electrodes were then washed with MES buffer, endotoxin-free water and dried in a gentle stream of Ar. Control experiments were also conducted by incubating an MUA-DPS/Au electrode with ODN-FITC and a TLR9/MUA-DPS/Au electrode with a blank sample, i.e. MES buffer. Fluorescence measurements were performed with an Olympus IX81confocal microscope and analyzed using cellSense imaging software.

3 Results and discussion

The preparation of mixed thiol SAMs for biosensor fabrication is typically carried out in two steps; first, a SAM of a long chain thiol is self-assembled on an electrode surface to covalently graft the biorecognition element, followed by backfilling with a short chain thiol blocking monolayer to fill up pinholes.[25] A one-step co-adsorption of a mixture of thiols to form mixed thiol SAMs is also recognized as an effective method in biosensor fabrication.[41,42] In this work, we followed the latter approach to tailor the molecular architecture layer. Scheme 1 shows the steps followed to fabricate the self-assembled TLR-based sensors. Two different approaches of forming co-adsorbed mixed thiol SAMs on Au electrodes were investigated and compared: self-assembly via passive incubation and potential-assisted deposition.

3.1 Self-assembly of mixed thiol SAMs by passive incubation

Clean, bare Au electrodes were first immersed in ethanolic solutions of MUA and MCH for 18 hours to create mixed thiol SAMs (MUA-MCH/Au). The mole ratio of the thiols ranged from 10–100% MUA and the total thiol concentration remained constant at 10 mM. The quality of the resulting SAM layers was examined using EIS in the presence of an [Fe(CN)$_6$]$^{3-/4-}$ redox probe. ESI Fig. S2† shows the Nyquist plots of a bare Au electrode, and Au electrodes after modification with different mole ratios of MUA and MCH forming MUA-MCH/Au surfaces. The

diameter of the semicircles of the curve, which is a measure of the charge transfer resistance (R_{CT}), increased with increasing the mole ratio of MUA. These results indicate that thicker SAMs (*i.e.* greater average chain length) exhibited greater resistance and are consistent with a previous work on R_{CT} *vs.* hydrocarbon chain length.[43] Following activation with EDC/NHS chemistry, the SAM modified electrodes were conjugated with TLR4 and the resulting surfaces' EIS was monitored using $[Fe(CN)_6]^{3-/4-}$. Attachment of TLR4 to the mixed thiol SAMs resulted in further increase of R_{CT} through the electrode surface. The fractional increase in ΔR_{CT}, shown in ESI Fig. S2b,† indicated that there were competing effects within the results. A greater amount of MUA resulted in more activation/attachment sites for TLR4 (10/90 *vs.* 50/50) while the longer-chain MUA molecule imparted greater overall R_{CT} to the SAM making it less responsive to the mass effects of the TLR4 biorecognition molecule (*viz.* 50/50 *vs.* 100/0). The thiol mixture of 25/75 provided the highest percentage response to covalent attachment of the TLR4 and was selected as the working ratio for subsequent studies. Since the longer chain thiol (MUA) is used to anchor the biorecognition element to the electrode surface and the shorter thiol (MCH) acts as a spacer tuning the distance among contiguous MUA molecules, this molar ratio should have provided the right steric environment for the optimal amount of TLR4 immobilized on MUA. At the lower molar ratio of 10 : 90, there may not be enough MUA on the Au surface to immobilize sufficient amount of TLR4. These results are consistent with previous studies with mixed MUA-MCH SAMs and immunoglobin used as the biorecognition molecules.[44,45]

3.2 Potential-assisted assembly of mixed thiol SAMs

Based on the above data (ESI Fig. S2b†), two separate mixed thiol (MUA-MCH and MUA-DPS) modified electrodes were prepared using the potential-assisted SAM deposition method described in the experimental section. The long chain MUA content was 25% by mole and the two shorter length thiols, MCH or DPS, were used as complementary thiols (75% by mole). The molar ratio of MCH and DPS with respect to MUA was kept the same in order to compare the antifouling properties of the short thiols when used at the same concentrations. ESI Fig. S3† shows the open circuit potential of a Au electrode initially decreased (cathodic shift) from ~50 mV to −200 mV (*vs.* Ag/AgCl) upon addition of the mixed thiol, indicating charge transfer from the mixed thiol to the Au electrode leading to Au–S bond formation.[26,27] The slow rise in potential from −200 mV to −50 mV over the next 4 hours is in agreement with the slow kinetics of the chemisorption of thiols under the commonly used open circuit potential (OCP) SAM deposition conditions.[26,27] Studies have shown that chemisorption of thiols on Au electrodes can be considered an oxidative process and applications of potentials greater than OCP can enhance the rate of adsorption of thiols, and generate better quality SAMs.[26,27] For potential-assisted deposition of mixed thiol SAMs, Au electrodes were submerged in mixed thiol solutions and biased to anodic potentials that are greater than open-circuit potentials (0.3–0.7 V) for 1–10 minutes, and the quality

of the resulting SAM layers was assessed *via* CV and EIS (data not shown). The surface coverage of SAMs deposited using an applied potential of +0.5 V (*vs.* Ag/AgCl) for 5 minutes was found to be optimal (>99% surface coverage).

Fig. 1a shows chronoamperometric deposition of mixed thiols of MUA-MCH and MUA-DPS using a potential of +0.5 V *vs.* Ag/AgCl, where the background current reached a minimum within 5 minutes of potential application. As shown in Fig. 1b, CV of a bare Au electrode showed a quasi-reversible redox reaction with a peak-to-peak separation (ΔE_p) of about ~100 mV while that of the mixed-thiol SAM modified surfaces showed near-complete elimination of the redox behavior at the electrode surface, suggesting successful formation of compact layers.

ESI Fig. S4† compares the Nyquist plots and CVs of $[Fe(CN)_6]^{3-/4-}$ using MUA-MCH/Au and MUA-DPS/Au surfaces (prepared *via* passive incubation and potential-assisted electrodeposition). Table 1 compares the charge transfer resistance and peak currents extracted from ESI Fig. S4.† From the table, it
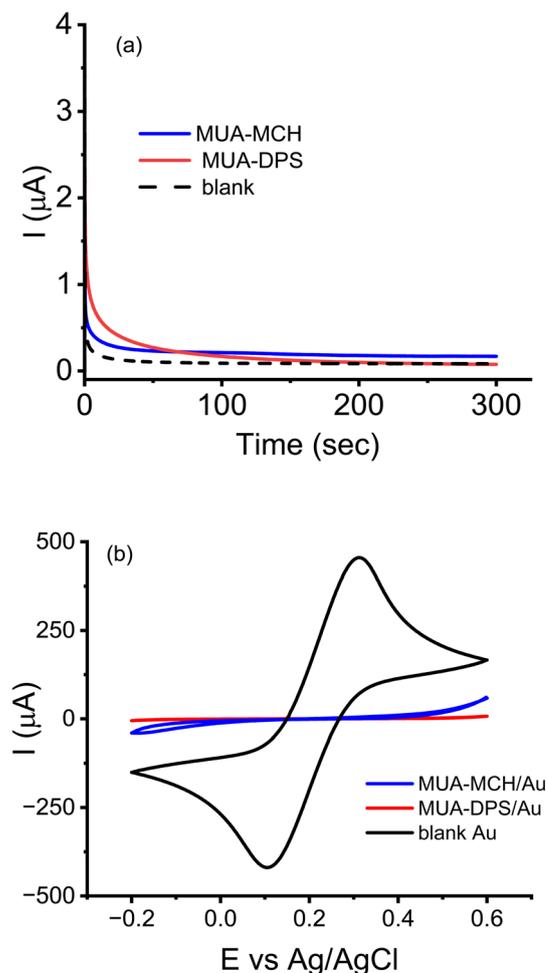

Fig. 1 (a) Chronoamperometry responses of mixed thiol deposition on Au electrodes held at +0.5 V *vs.* Ag/AgCl in a solution containing MUA-MCH and MUA-DPS; (b) CVs of 1 mM $[Fe(CN)_6]^{3-/4-}$ in 0.1 M PBS, pH 7.4 using a bare Au and electrodeposited MUA-MCH and MUA-DPS SAMs modified Au electrodes.

Table 1 EIS, CV and surface coverage for mixed thiol SAMs on Au electrodes^a

	MUA-MCH		MUA-DPS	
	EIS	CV	EIS	CV
	R_{CT} (kΩ) ($n = 4$)	I_{peak} (μA)	R_{CT} (kΩ) ($n = 4$)	I_{peak} (μA)
Bare Au	0.196 ± 0.022	451	0.203	476
Passive incubation	48.3 ± 2.1	10.3	177.7 ± 31.3	1.31
Potential-assisted deposition	61.9 ± 1.8	3.9	182.3 ± 15.9	1.07
θ by passive incubation	99.61%	97.80%	99.88%	99.76%
θ by potential-assisted deposition	99.84%	99.15%	99.90%	99.79%

^{a} θ = fractional SAM surface coverage.

is evident that the R_{CT} values of electrodeposited SAMs were slightly greater than the R_{CT} of the same mole fraction SAMs prepared by passive incubation. The slightly enhanced passivation of electrode surfaces under electrodeposition conditions could be due to reduced number of defect sites. Also, the table shows that SAMs containing the zwitterionic thiol DPS exhibited significantly greater R_{CT} than the non-ionic MCH, which could be due to electrostatic repulsion between the negatively charged redox probe and DPS. Similar observations were made from the CV data where the peak currents of the redox probe were reduced by ∼400 times for MUA-DPS modified electrodes and by ∼100 times for the MUA-MCH modified electrodes. From the change in R_{CT} and peak current values shown in Table 1, we calculated the fractional surface coverage (θ) of the electrodes by mixed thiol SAMs to be >98% [$\theta = 1 - (I_p^{SAM}/I_p^{bare}) = 1 - (R_{CT}^{bare}/R_{CT}^{SAM})$ where I_p and R_{CT} have their usual meanings]. From these data, it is apparent that the rapid potential-assisted deposition of SAMs (5 minutes, +0.5 V) provides insulating layers on Au electrodes that are comparable to passive incubation (18 hours) – a decrease in SAM formation time by >200-fold. In fact, the potential-assisted SAM deposition method showed superior reproducibility compared to the passive incubation method, as evidenced in the lower coefficient of variance (relative standard deviation, $n = 3$) of the measured R_{CT} values: 2.9% and 4.3% for MUA-MCH/Au vs. 8.7% and 17.6% for MUA-DPS/Au.

We also conducted linear sweep voltammetry (LSV) for reductive desorption of electrodeposited MUA-DPS/Au and MUA-MCH/Au SAMs to obtain quantitative information about surface coverage by the SAM layers (ESI Fig. S5†). The reductive desorption peak potentials observed at ∼−0.91 V and ∼−0.93 V for the MUA-DPS and MUA-MCH SAMs, respectively, suggest that homogeneously mixed SAMs were obtained using potential-assisted deposition of the mixed thiols prepared in the solvents used in this work at room temperature. Integrating the charges associated with the reductive currents of the mixed thiol SAMs gave average values ($n = 3$) of 61.79 ± 9.13 μC cm^{-2} and 68.85 ± 9.01 μC cm^{-2} for the MUA-DPS/Au and MUA-MCH/Au electrodes, respectively, with thiol surface coverages of (6.4 ± 0.95) × 10^{-10} mol cm^{-2} and (7.13 ± 0.93) × 10^{-10} mol cm^{-2}. These values are similar to typical literature reported values for compact SAM structures.[38,46] A control LSV experiment for a bare

Au electrode, ESI Fig. S5,† showed a cathodic peak at a reductive potential <−1.1 V, which is ascribed to the evolution of H$_2$ gas.

XPS analysis was also used to further characterize the deposition of mixed thiol SAMs on Au surfaces. High resolution XPS spectra for MUA-MCH/Au and MUA-DPS/Au surfaces are shown in ESI Fig. S6.† The spectra show similar features in both passive incubation and potential-assisted deposition preparations, each displaying a broad XPS signal at ∼162 eV, indicating thiols bound to the Au surface. The S$_{2p}$ signal was fitted with a doublet peak at 162.0 eV and 163.5 eV, which are characteristic of S$_{2p3/2}$ and S$_{2p1/2}$ peaks associated with the Au-thiol bond. There were minimal contributions from unbound thiols as evidenced by the small doublets seen above 163 eV. In addition, the prominent peak at ∼168 eV for the MUA-DPS/Au spectra was assigned to the SO$_3^{2-}$ residue of sulfobetaine.[47] For the MUA-MCH/Au samples, the weak signals observed above 166 eV are assigned to oxidized sulphur species as these samples were stored under ambient conditions over two weeks prior to XPS analysis. These XPS spectra are consistent with the EIS and CV experiments whereby rapid potential-assisted SAM formation provides high quality thiol layers for electrochemical sensor fabrication.

3.3 Characterization of TLR biosensors

Prior to assembling the TLR sensors on the mixed thiol SAM modified Au electrodes, we evaluated the antifouling properties of electrodeposited/MUA-DPS/Au and MUA-MCH/Au surfaces using BSA as a model protein. ESI Fig. 7† shows the change in EIS responses of TLR4 biosensors (TLR4/MUA-MCH/Au and TLR4/MUA-DPS/Au electrodes) exposed to a freshly prepared 1 mg mL^{-1} BSA solution for 1 h. After BSA exposure, the %ΔR_{CT} of the TLR4/MUA-MCH/Au surface increased by 20.3 ± 1.3% ($n = 4$), whereas the TLR sensor constructed on MUA-DPS/Au exhibited a %ΔR_{CT} of only 1.6 ± 1.0 % ($n = 4$), showing superior anti-fouling properties of the zwitterionic DPS. This is consistent with literature reports of ultralow-fouling properties of other zwitterionic sulfobetaine compounds in biosensor fabrication.[32,34,48] Thus, electrochemically deposited MUA-DPS SAMs on Au electrodes were used to construct the TLR sensors below.

Fig. 2a shows the CVs of the major steps in Scheme 1 for the TLR4 sensor preparation on the MUA-DPS/Au electrode. The
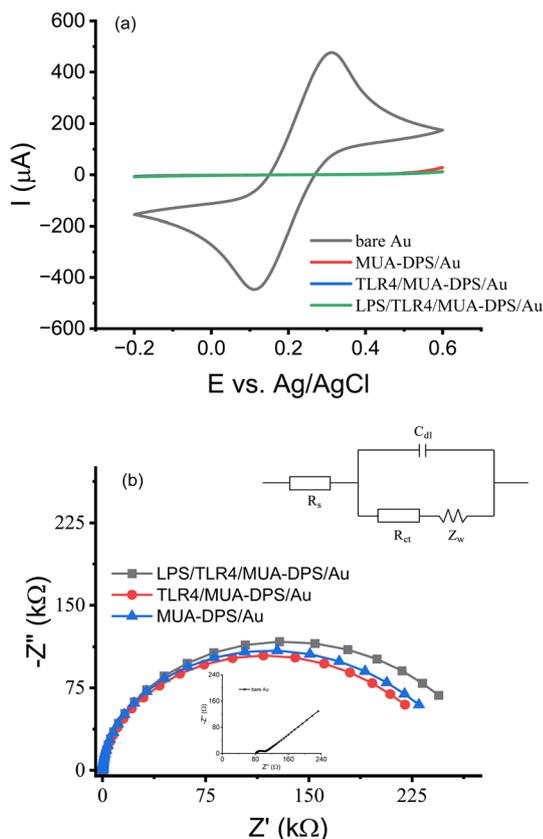
Fig. 2 Cyclic voltammograms (a) and Nyquist plots (b) of the Au electrode following the steps in TLR sensor fabrication using 1 mM $[Fe(CN)_6]^{3-/4-}$ prepared in PBS buffer (pH = 7.4). Inset in (b) also shows the Randles equivalent circuit used for all fits. R_s is the solution resistance; C_{dl} is the electrode double layer capacitance; Z_w is the Warburg impedance and R_{CT} is the charge transfer resistance at the electrode interface.

bare Au electrode shows the distinctive redox peaks of $[Fe(CN)_6]^{3-/4-}$ similar to Fig. 1b. Electrodeposition of the MUA-DPS SAM provided almost complete elimination of the redox reaction on the electrode surfaces. Subsequent covalent attachments of TLR4 and its target analyte (LPS) induced negligible decrease to the redox reaction on the already passivated surface. The corresponding Nyquist plot of the various modified surfaces is shown in Fig. 2b; the inset in Fig. 2b shows the Randles equivalent circuit[49] to which the impedance data were fitted to obtain the circuit element values of the modified electrodes shown in Table 2. The quality of the data fit to the equivalent circuit was weighed by a goodness of fit value of <0.002. The Nyquist plot of a bare Au electrode showed

Table 2 Evaluation of parameters from the Nyquist plot in Fig. 2b using the Randles equivalent circuit model on a Au electrode

Electrode surface	R_s (Ω)	R_{CT} (kΩ)	C_{dl} (μF)	W (S·s$^{1/2}$)
Au	90.18	0.155	10.03	7.32×10^{-3}
MUA-DPS/Au	95.84	174.9	1.361	1.77×10^{-5}
TLR4/MUA-DPS/Au	89.60	193.4	1.296	2.13×10^{-5}
LPS/TLR4/MUA-DPS/Au	94.49	215.8	1.220	1.96×10^{-5}

an almost straight 45° line with a calculated R_{CT} of 155 Ω and an electrical double layer capacitance (C_{dl}) of 10.03 μF, which stem from the Warburg impedance and imply a diffusion limited electrochemical process. The Nyquist plot of MUA-DPS/Au shows a well-defined semicircle with an R_{CT} of 174.9 kΩ and C_{dl} of 1.361 μF. The significant increase in R_{CT} and decrease in C_{dl} of the MUA-DPS/Au *vs.* the bare Au electrode confirmed the potential-assisted assembly of MUA-DPS on the Au electrode, which inhibited the diffusion of the redox probe to the electrode surface and increased the double layer thickness. Subsequent attachment of the TLR and LPS layers resulted in a noticeable increase in R_{CT} and a decrease in C_{dl}, indicating the successful fabrication of the TLR4 sensor on the electrodeposited MUA-DPS/Au surface.

Both MUA-DPS/Au and TLR4/MUA-DPS/Au electrode surfaces were characterized by XPS to confirm the attachment of the protein to the SAM layer. As shown in ESI Fig. S8,† the MUA-DPS layer exhibited a N 1s peak at 402 eV due to the quaternary ammonium group in DPS. Upon binding with the TLR, a broad N 1s peak at 400 eV was detected which is assigned to peptide bonds.[50] The broad C 1s peaks at 286–290 eV were assigned to the protein's amine groups (C–NH, 286.6 eV), peptide bonds (C=O–NH, 288.2 eV) and carboxylic groups (C–OO$^-$, 289.0 eV), confirming the immobilization of TLR molecules on the SAM modified electrode surface.

The binding and surface coverage of TLR on the MUA-DPS/Au electrode were also determined using QCM as described in the Methods section. The response of the QCM to the covalent attachment of TLR4 during a 4 hour incubation is shown in Fig. 3. Prior to adding the TLR4 solution, the static QCM cell was equilibrated with PBS buffer and a stable baseline with a Δf of ±0.76 Hz for 180 seconds was recorded. While continuously monitoring the QCM response, a 250 μL solution of TLR4 (in PBS buffer) was added to the cell to obtain a final solution concentration of TLR4 of 5 μg mL^{-1}. After TLR4 addition, the resonance frequency decreased indicating binding of TLR4 on
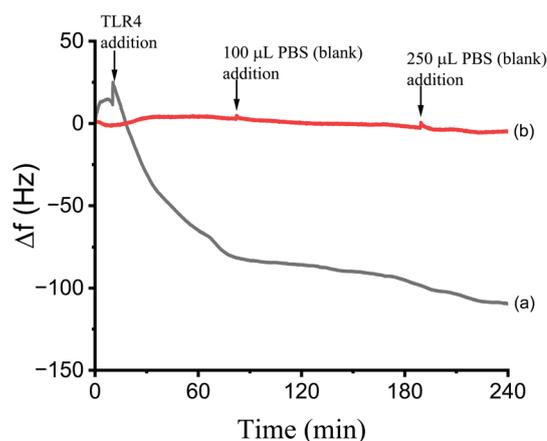

Fig. 3 QCM response showing (a) TLR4 binding on a MUA-DPS mixed thiol modified Au electrode equilibrated in PBS (pH = 7.4) buffer, and (b) control experiments using a clean Au QCM electrode kept in the static cell with PBS (pH = 7.4) solution after the addition of 100 μL and 250 μL PBS buffer.

the mixed thiol SAM surface, and reached a plateau with a net frequency change of 123 Hz after ~4 hours. Control experiments with adding PBS buffer alone showed negligible change in Δf (Fig. 3). Using the Sauerbrey equation[46] and the net frequency change observed after TLR4 addition, we calculated the mass of the TLR4/MD2 complex on the MUA-DPS/Au surface to be 1705 ng cm^{-2}. For a predicted total molecular mass of 89.8 kDa for the TLR4/MD2 complex, this frequency change corresponds to a surface concentration of 0.19×10^{-10} mol cm^{-2} or 1.14×10^{13} molecules per cm^2. This value is similar to what has been reported for proteins immobilized on thiol modified gold electrodes.[51,52]

3.4 TLR4 biosensor for detection of LPS

LPS, which is a cell wall component of Gram-negative bacteria, is a serologically reactive bacterial toxin with a lethal dose in humans as low as 1 to 2 µg,[53] and monitoring its content in various samples including biofluids, food, air, water and soil is important for epidemiology, the environment, and disease control and treatment.[54] The EIS signal of the TLR4 sensor was determined for a range of concentrations of LPS (10–1000 ng mL^{-1}) and is shown in Fig. 4a. Each data point represents an average of 3 sensors prepared and processed in parallel. The semilogarithmic plot shows linearity over two orders of magnitude. The theoretical limit of detection (LOD) was estimated to be 4 ng mL^{-1}, estimated as the mean baseline response (%ΔR_{CT} for blank) plus three times the standard deviation of the blank. The LOD achieved in this work is superior to what has been reported for EIS detection of LPS using TLR4 on a planar Au electrode (WE 0.02 cm^2, LOD 35 ng mL^{-1}),[19] and is comparable to those using planar Au electrodes (WE 0.5 cm^2, LOD 1 ng mL^{-1})[13] and nanoporous ITO electrodes (LOD 2 ng mL^{-1}),[14] and is within the toxicologically relevant concentration of LPS.[54,55] Amini et al.[11] and Mayall et al.[18] reported LODs of ~1.3×10^{-4} EU mL^{-1} (approximately 2.6×10^{-5} ng mL^{-1}) for lysed E. Coli and lysed Salmonella typhimurium, respectively, using larger planar Au electrodes (WE 0.5 cm^2) and signal amplification techniques; however the dynamic ranges of these sensors are limited to ~5 EU mL^{-1} (approximately 1 ng mL^{-1}). The response of our sensor to a non-analyte (flagellin protein from Salmonella typhimurium, 10 and 1000 ng mL^{-1}), noted in red squares, showed a minor increase in background signal which was not concentration dependent within experimental error, demonstrating the selectivity of the sensor.

The TLR4 sensor was also challenged with samples of LPS (1000 ng mL^{-1}) spiked into human blood plasma samples as shown in Fig. 4b. The presence of plasma modified the signal by ~15% compared to LPS in buffer alone. These results demonstrate the zwitterionic antifouling component, DPS, is effective in minimizing non-specific adsorption of biofoulants on the TLR4 biosensor, enabling LPS detection in human blood plasma samples. This demonstrates the robustness of such sensors for the determination of target analytes in real world samples.

We also studied the shelf-life stability of parallelly prepared TLR4/MUA-DPS/Au sensors and stored in PBS buffer (pH 7.4) at
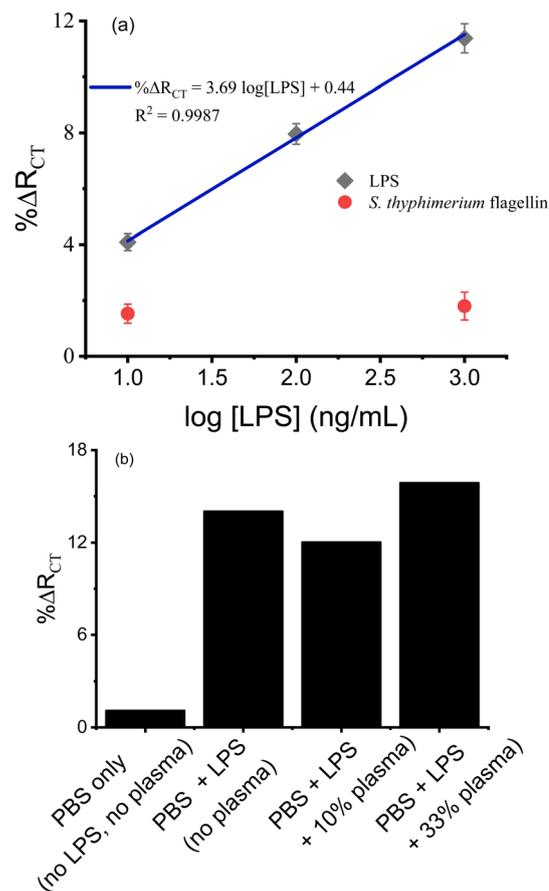

Fig. 4 (a) Dose–response curve of TLR4/MUA-DPS/Au towards LPS. Response of the sensor towards control samples (10 and 1000 ng mL^{-1} flagellin from Salmonella typhimurium) is shown with red circles; (b) the response of the TLR4 sensor (TLR4/MUA-DPS/Au) for 1000 ng mL^{-1} LPS spiked pooled human blood plasma samples. The data points and error bars represent the mean and standard deviation of three independent sensors fabricated and processed in parallel.

4 °C for 3 weeks. ESI Fig. S9† shows that TLR4 sensors exposed to 1000 ng mL^{-1} LPS retained ~80% of their initial response after 7 days of storage, but displayed only ~50% of their initial response after 21 days of storage. The deterioration of the sensor performance after storage for extended time is possibly due to slow degradation of the SAM layer causing loss of TLR4 from the sensor electrode and/or reduced binding affinity of the TLR4 protein to its ligand, LPS, upon storage. She et al.[12] noted a similar decrease in sensor response for TLR5 biosensors stored in PBS (pH 7.4) buffer at 4 °C for up to 14 days, which the authors ascribed to slow dissociation of TLR5 protein from the sensor surface. Despite the challenges with the long-term stability of alkanethiol-based sensors, they remain some of the most studied interfacial materials in sensor development.[56] The storage stability of proteins (immunosensors) in the layers of SAMs is also affected by the microenvironment they are in, limiting their storage stability to days under refrigeration and wet conditions.[57] Hence, the rapid and facile sensor fabrication method reported in this work could be beneficial for onsite and on-demand sensor fabrication, when sensors cannot be

fabricated beforehand and stored. In recent reports, Mayall *et al.*[58] and Singh *et al.*[15] have shown that biosensors fabricated *via* passive incubation of electrodes using N-heterocyclic carbenes (NHC) as linker molecules rendered extended storage stability (up to 4 weeks) in buffer at 4 °C, without losing significant sensor performance. Similar storage stability (4 weeks) was also reported for TLR4 sensors using glutaraldehyde as a linker molecule on carbon nanotube modified electrodes.[16] The authors attributed the improved storage stability of their biosensors to the robustness and stability of NHC SAMs and glutaraldehyde when stored in buffers at 4 °C.

3.5   Detection of CpG ODN by TLR9 biosensors

The binding of CpG ODN on the TLR9/MUA-DPS/Au electrode was first assessed *via* fluorescence microscopy using a fluorescein isothiocyanate (FITC) tagged CpG ODN. Negative control experiments, *i.e.*, without TLR9 or FITC CPG ODN exposure, were also designed and conducted under the same conditions. Fig. 5a and b show the fluorescence microscopy images of TLR9/MUA-DPS/Au sensors exposed to 10 and 50 $\mu g\ mL^{-1}$ FITC-CPG ODN, respectively, displaying green fluorescence responses whereas the control samples (Fig. 5c and d) do not show any fluorescence signals. These results confirm the binding of TLR9 with CpG ODN under the experimental conditions described in the Methods section.

The performance of the TLR9/MUA-DPS/Au electrode was then determined against varying concentrations of the target CpG ODN (10–350 $\mu g\ mL^{-1}$) *via* EIS. The TLR9-CpG ODN interactions were performed at pH 5.5 in MES buffer since the receptor–ligand binding favours slightly acidic conditions.[9,39] (Similarly, the EIS measurements were performed with 1 mM $Fe(CN)_6^{3-/4-}$ prepared in 0.1 M KNO_3, instead of the slightly alkaline PBS that we used for the TLR4 sensor characterization.) The resulting Nyquist plot shown in Fig. 6a displays an increase in the diameter of the semicircles as the concentration of ODN increased, implying a higher amount of the analyte was bound to the TLR9 sensor. The values of %ΔR_{CT} of the sensor are plotted as a dose response curve in Fig. 6b (black diamond), showing a logarithmic linear relationship in the clinically relevant CpG ODN concentration range.[36,59] Each data point is an average of three independent sensors prepared and processed in parallel, with the error bars showing the standard deviations of the measurements. The theoretical LOD was calculated to be 7 $\mu g\ mL^{-1}$, calculated as $3\sigma_{blank}$ plus %ΔR_{CT} blank. While the LOD of our sensor is similar to that of the only literature reported TLR9 CpG ODN impedimetric sensor (5 $\mu g\ mL^{-1}$),[17] the dynamic range is superior (<20 $\mu g\ mL^{-1}$ reported in ref. 17). The class specificity of the sensor was also examined using two different non-target materials (a non-binding ODN and LPS) as negative controls. Fig. 6b (open star and triangle) shows the sensor exhibits negligible response to the negative controls, demonstrating the high selectivity of the sensor.

Electrode reusability can be a desired attribute when developing practical sensors that require time consuming electrode fabrication procedures. In this work, we employed our previously reported electrochemical reductive desorption technique
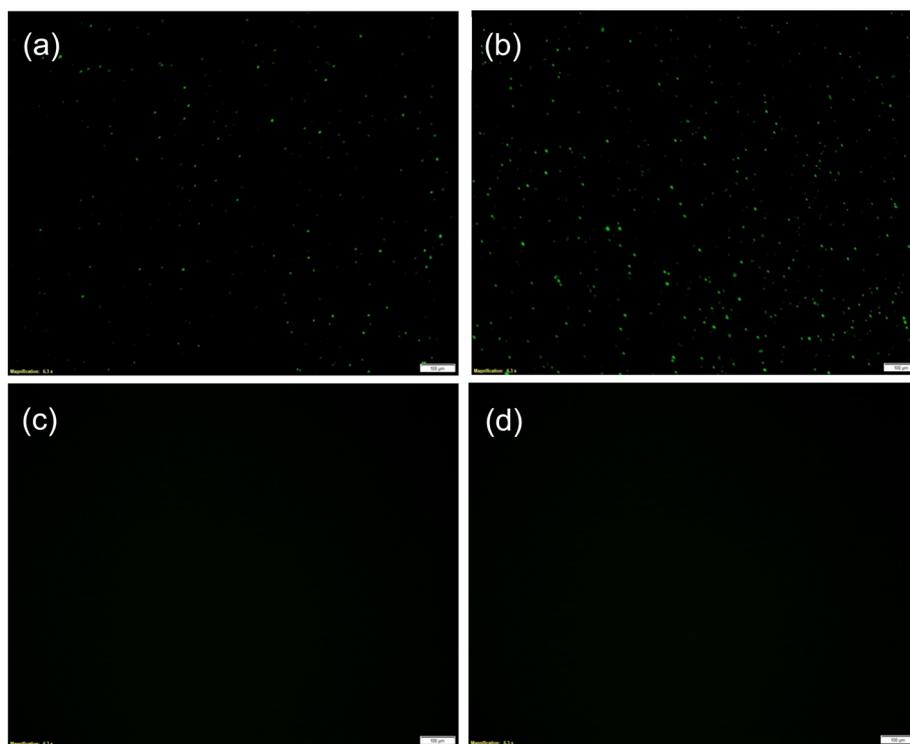

Fig. 5   Fluorescence microscopy images (magnification 10×) of the TLR9/MUA-DPS/Au sensor exposed to (a) 10 $\mu g\ mL^{-1}$ FITC CpG-ODN and (b) 50 $\mu g\ mL^{-1}$ FITC CpG-ODN. (c) A control experiment where an MUA-DPS/Au electrode incubated with 50 $\mu g\ mL^{-1}$ FITC CpG-ODN and (d) TLR9/MUA-DPS/Au sensor incubated with buffer alone. Scale bars represent 100 μm.
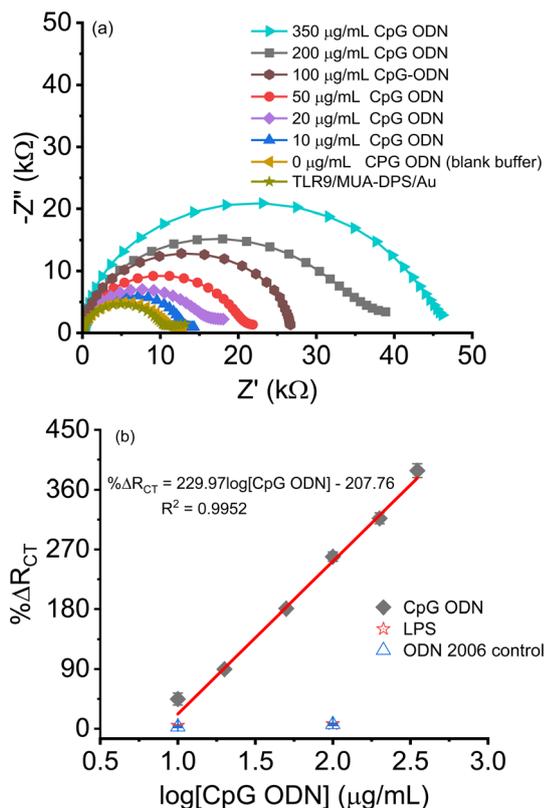
Fig. 6 (a) Nyquist plot of the TLR9/MUA-DPS/Au sensor after 30 minute incubation with various concentrations of CpG ODN. The amount of CpG ODN (μg mL^{-1}) used to generate each EIS data point is indicated in the plot; (b) calibration plot of %ΔR_{CT} of the TLR9 biosensor as a function of logarithm of CpG ODN concentration. Data points and error bars represent the mean and standard deviation of three independent sensors fabricated and processed in parallel.

to repeatedly desorb and self-assemble the TLR sensors.[38,40] Previously, we have shown that an electrochemical desorption technique can be used to rebuild aptasensors and immunosensors, using passively self-assembled 1,6-hexanedithiol as a linker molecule, up to 30 times on the same Au electrode without losing sensor performance.[38,40] Using a similar strategy, we used a single Au WE at least 5 times to desorb and rebuild TLR9 sensors. ESI Fig. S10† compares CV and EIS of $[Fe(CN)_6]^{3-/4-}$ using freshly fabricated and regenerated Au electrodes. After 5 cycles of TLR9 sensor assembly and desorption over several days, regenerated Au electrodes retained >96% of both their initial current and total charge. The EIS data is also in agreement with the CV observation whereby the impedance spectrum of the regenerated electrode is similar to that of the freshly prepared Au electrode (RSD of R_{CT} = 3.5%, n = 5).

4 Conclusions

The work presented herein demonstrates rapid and facile fabrication of TLR biosensors using potential-assisted self-assembly of mixed thiols for EIS detection of microbial pathogen components. Compared to passive incubation of mixed alkanethiols, application of a modest anodic potential to gold electrodes facilitated the chemisorption of thiols for SAM formation, reducing the sensor fabrication time by more than 200-fold. A SAM of a binary mixture of MUA and an in-house synthesized zwitterionic thiol, DPS, demonstrated superior antifouling performance compared to the commonly used binary mixture of MUA and MCH at an equal molar ratio. Different MUA-DPS/Au electrodes were modified with TLR4 and TLR9 proteins and used for sensitive EIS detection of LPS and CpG ODN, respectively, over a broad range of concentrations (>10^2) with low detection limits (4 ng mL^{-1} for TLR4-LPS and 7 μg mL^{-1} for TLR9-CPG ODN). The low limits of detection and short sensor fabrication time presented in this work compare favorably (5 minutes for SAM formation) with other reports of TLR-based EIS sensors, where SAM formation alone typically required in excess of 48 hours. The response of a TLR4/MUA-DPS/Au sensor for LPS in the presence of up to 33% human blood plasma was not significantly affected by the matrix, indicating the sensor can be used in real-world sample analysis. TLR9 sensors show a promising response towards CpG ODN, showing its potential to identify bacterial and viral DNAs. However, like all alkanethiol-based biosensors, the TLR/MUA-DPS/Au sensors were found to have a limited shelf-life time when stored in a buffer at 4 °C and retained only ~50% of their initial response after 3 weeks of storage. Thus, rapid assembly of the sensor and reusability of the gold working electrode could be advantageous when sensors can't be fabricated in advance and stored for a long time. Here, we show that working Au electrodes could be regenerated using an electrochemical reductive desorption technique, and a single Au electrode could be assembled with the complete sensor molecular architecture and disassembled at least 5 times with minimal degradation in electrochemical performance (%RSD < 8%). These results provide significant insight towards future development of onsite-assembled, field-deployable biosensor platforms that could potentially be used for early warning and diagnosis of pathogen contamination in clinical, food and environmental samples.

Data availability

The data supporting this article have been included as part of the ESI.†

Author contributions

Rajesh G. Pillai: writing – original draft, investigation, data curation and analysis. Khalid Azyat: synthesis of the sulfobetaine, ^{1}H NMR and data analysis. Nora W. C. Chan: writing – review & editing, project administration, funding acquisition, conceptualization. Abebaw B. Jemere: writing – review & editing, supervision, resources, project administration, methodology, funding acquisition, formal analysis, conceptualization.

Conflicts of interest

The authors declare that they have no competing interests.

Acknowledgements

References

1 O. Lazcka, F. J. D. Campo and F. X. Muñoz, Pathogen detection: A perspective of traditional methods and biosensors, *Biosens. Bioelectron.*, 2007, **22**(7), 1205–1217.

2 M. Sharafeldin and J. J. Davis, Point of Care Sensors for Infectious Pathogens, *Anal. Chem.*, 2021, **93**(1), 184–197.

3 S. A. Walper, *et al.*, Detecting Biothreat Agents: From Current Diagnostics to Developing Sensor Technologies, *ACS Sens.*, 2018, **3**(10), 1894–2024.

4 D. Metzgar, *et al.*, The value and validation of broad spectrum biosensors for diagnosis and biodefense, *Virulence*, 2013, **4**(8), 752–758.

5 M. Naseri, *et al.*, Rapid Detection of Gram-Positive and -Negative Bacteria in Water Samples Using Mannan-Binding Lectin-Based Visual Biosensor, *ACS Sens.*, 2022, **7**(4), 951–959.

6 A. D. Cabral, *et al.*, Sensitive Detection of Broad-Spectrum Bacteria with Small-Molecule Fluorescent Excimer Chemosensors, *ACS Sens.*, 2020, **5**(9), 2753–2762.

7 D. Metzgar, *et al.*, Broad-spectrum biosensor capable of detecting and identifying diverse bacterial and Candida species in blood, *J. Clin. Microbiol.*, 2013, **51**(8), 2670–2678.

8 R. M. Martinez, *et al.*, Evaluation of three rapid diagnostic methods for direct identification of microorganisms in positive blood cultures, *J. Clin. Microbiol.*, 2014, **52**(7), 2521–2529.

9 M. Rutz, *et al.*, Toll-like receptor 9 binds single-stranded CpG-DNA in a sequence- and pH-dependent manner, *Eur. J. Immunol.*, 2004, **34**(9), 2541–2550.

10 T. Y. Yeo, *et al.*, Electrochemical endotoxin sensors based on TLR4/MD-2 complexes immobilized on gold electrodes, *Biosens. Bioelectron.*, 2011, **28**(1), 139–145.

11 K. Amini, *et al.*, Characterization of TLR4/MD-2-modified Au sensor surfaces towards the detection of molecular signatures of bacteria, *Anal. Methods*, 2016, **8**(42), 7623–7631.

12 Z. She, *et al.*, Investigation of the utility of complementary electrochemical detection techniques to examine the *in vitro* affinity of bacterial flagellins for a toll-like receptor 5 biosensor, *Anal. Chem.*, 2015, **87**(8), 4218–4224.

13 R. M. Mayall, *et al.*, An electrochemical lipopolysaccharide sensor based on an immobilized Toll-Like Receptor-4, *Biosens. Bioelectron.*, 2017, **87**, 794–801.

14 D. Lin, *et al.*, Nanostructured indium tin oxide electrodes immobilized with toll-like receptor proteins for label-free electrochemical detection of pathogen markers, *Sens. Actuators, B*, 2018, **257**, 324–330.

15 I. Singh, *et al.*, N-Heterocyclic carbenes meet toll-like receptors, *Chem. Commun.*, 2021, **57**(68), 8421–8424.

16 R. Gangwar, *et al.*, Toll-like receptor-immobilized carbon paste electrodes with plasma functionalized amine termination: Towards real-time electrochemical based triaging of gram-negative bacteria, *Biosens. Bioelectron.*, 2023, **241**, 115674.

17 D. S. Lee, *et al.*, Toll like receptor-based electrochemical sensors *via* N-heterocyclic carbene-modified surfaces: towards improved sensing of DNA molecules, *Mater. Adv.*, 2024, **5**, 6063–6069.

18 R. M. Mayall, *et al.*, Enhanced Signal Amplification in a Toll-like Receptor-4 Biosensor Utilizing Ferrocene-Terminated Mixed Monolayers, *ACS Sens.*, 2019, **4**(1), 143–151.

19 R. P. S. de Campos, *et al.*, An integrated digital microfluidic electrochemical impedimetric lipopolysaccharide sensor based on toll-like receptor-4 protein, *Biosens. Bioelectron.: X*, 2024, **16**, 100433.

20 M. S. Mannoor, *et al.*, Electrical detection of pathogenic bacteria *via* immobilized antimicrobial peptides, *Proc. Natl. Acad. Sci. U. S. A.*, 2010, **107**(45), 19207–19212.

21 E. Tenenbaum and E. Segal, Optical biosensors for bacteria detection by a peptidomimetic antimicrobial compound, *Analyst*, 2015, **140**(22), 7726–7733.

22 J. R. Uzarski and C. M. Mello, Detection and Classification of Related Lipopolysaccharides *via* a Small Array of Immobilized Antimicrobial Peptides, *Anal. Chem.*, 2012, **84**(17), 7359–7366.

23 K. A. Fitzgerald and J. C. Kagan, Toll-like Receptors and the Control of Immunity, *Cell*, 2020, **180**(6), 1044–1066.

24 D. Capitao, *et al.*, On the decisive role of the sulfur-based anchoring group in the electro-assisted formation of self-assembled monolayers on gold, *Electrochim. Acta*, 2017, **257**, 165–171.

25 J. J. Gooding and N. Darwish, The rise of self-assembled monolayers for fabricating electrochemical biosensors—an interfacial perspective, *Chem. Rec.*, 2012, **12**(1), 92–105.

26 F. Ma and R. B. Lennox, Potential-Assisted Deposition of Alkanethiols on Au: Controlled Preparation of Single- and Mixed-Component SAMs, *Langmuir*, 2000, **16**(15), 6188–6190.

27 R. G. Pillai, M. D. Braun and M. S. Freund, Electrochemically Assisted Self-Assembly of Alkylthiosulfates and Alkanethiols on Gold: The Role of Gold Oxide Formation and Corrosion, *Langmuir*, 2010, **26**(1), 269–276.

28 D. Jambrec, *et al.*, Potential-Pulse-Assisted Formation of Thiol Monolayers within Minutes for Fast and Controlled Electrode Surface Modification, *ChemElectroChem*, 2016, **3**(9), 1484–1489.

29 M. Casian, *et al.*, Electrochemically assisted DNA and thioaromatic assembly as sensing and antifouling interface for food allergens, *Microchim. Acta*, 2024, **191**(2), 97.

30 K. K. Leung, *et al.*, Measuring and Controlling the Local Environment of Surface-Bound DNA in Self-Assembled

Monolayers on Gold When Prepared Using Potential-Assisted Deposition, *Langmuir*, 2020, **36**(24), 6837–6847.

31 D. Blasi, *et al.*, Enhancing the Sensitivity of Biotinylated Surfaces by Tailoring the Design of the Mixed Self-Assembled Monolayer Synthesis, *ACS Omega*, 2020, **5**(27), 16762–16771.

32 Y. S. Wang, *et al.*, Functional Biointerfaces Based on Mixed Zwitterionic Self-Assembled Monolayers for Biosensing Applications, *Langmuir*, 2019, **35**(5), 1652–1661.

33 I. I. Suni, Substrate Materials for Biomolecular Immobilization within Electrochemical Biosensors, *Biosensors*, 2021, **11**(7), 239.

34 Q. Li, *et al.*, Zwitterionic Biomaterials, *Chem. Rev.*, 2022, **122**(23), 17073–17154.

35 T. Gosiewski, *et al.*, Comprehensive detection and identification of bacterial DNA in the blood of patients with sepsis and healthy volunteers using next-generation sequencing method - the observation of DNAemia, *Eur. J. Clin. Microbiol. Infect. Dis.*, 2017, **36**(2), 329–336.

36 A. Dalpke, *et al.*, Activation of Toll-Like Receptor 9 by DNA from Different Bacterial Species, *Infect. Immun.*, 2006, **74**(2), 940–946.

37 H. S. Kim, *et al.*, Separation of Olefin/Paraffin Mixtures Using Zwitterionic Silver Complexes as Transport Carriers, *Chem. – Eur. J.*, 2007, **13**(9), 2655–2660.

38 A. M. Mahmoud, *et al.*, A regenerating self-assembled gold nanoparticle-containing electrochemical impedance sensor, *Biosens. Bioelectron.*, 2014, **56**, 328–333.

39 J. Vollmer and A. M. Krieg, Immunotherapeutic applications of CpG oligodeoxynucleotide TLR9 agonists, *Adv. Drug Delivery Rev.*, 2009, **61**(3), 195–204.

40 D. Lin, *et al.*, A regenerating ultrasensitive electrochemical impedance immunosensor for the detection of adenovirus, *Biosens. Bioelectron.*, 2015, **68**, 129–134.

41 R. Meunier-Prest, *et al.*, Potential-assisted deposition of mixed alkanethiol self-assembled monolayers, *Electrochim. Acta*, 2010, **55**(8), 2712–2720.

42 L. Sarcina, *et al.*, Controlling the Binding Efficiency of Surface Confined Antibodies through the Design of Mixed Self-Assembled Monolayers, *Adv. Mater. Interfaces*, 2023, **10**(12), 2300017.

43 A. Sharma, *et al.*, Electrochemical impedance spectroscopy study of carbohydrate-terminated alkanethiol monolayers on nanoporous gold: Implications for pore wetting, *J. Electroanal. Chem.*, 2016, **782**, 174–181.

44 J. S. Cisneros, *et al.*, Electrochemical impedance biosensor for Chagas Disease diagnosis in clinical samples, *Biosens. Bioelectron.: X*, 2022, **12**, 100261.

45 K. Tsugimura, *et al.*, Protein-G-based human immunoglobulin G biosensing by electrochemical impedance spectroscopy, *Jpn. J. Appl. Phys.*, 2016, **55**(2S), 02BE06.

46 T. Bertok, *et al.*, Mixed Zwitterion-Based Self-Assembled Monolayer Interface for Impedimetric Glycomic Analyses of Human IgG Samples in an Array Format, *Langmuir*, 2016, **32**(28), 7070–7078.

47 T. Bertok, *et al.*, Ultrasensitive Impedimetric Lectin Biosensors with Efficient Antifouling Properties Applied in Glycoprofiling of Human Serum Samples, *Anal. Chem.*, 2013, **85**(15), 7324–7332.

48 Z. Xu, *et al.*, Electrochemical biosensors for the detection of carcinoembryonic antigen with low fouling and high sensitivity based on copolymerized polydopamine and zwitterionic polymer, *Sens. Actuators, B*, 2020, **319**, 128253.

49 M. Banakar, *et al.*, Electrochemical Biosensors for Pathogen Detection: An Updated Review, *Biosensors*, 2022, **12**(11), 927.

50 S. Ray and A. G. Shard, Quantitative Analysis of Adsorbed Proteins by X-ray Photoelectron Spectroscopy, *Anal. Chem.*, 2011, **83**(22), 8659–8666.

51 H. T. Phan, *et al.*, Investigation of Bovine Serum Albumin (BSA) Attachment onto Self-Assembled Monolayers (SAMs) Using Combinatorial Quartz Crystal Microbalance with Dissipation (QCM-D) and Spectroscopic Ellipsometry (SE), *PLoS One*, 2015, **10**(10), e0141282.

52 S. Boujday, *et al.*, In-Depth Investigation of Protein Adsorption on Gold Surfaces: Correlating the Structure and Density to the Efficiency of the Sensing Layer, *J. Phys. Chem. B*, 2008, **112**(21), 6708–6715.

53 M. M. Dinges and P. M. Schlievert, Comparative analysis of lipopolysaccharide-induced tumor necrosis factor alpha activity in serum and lethality in mice and rabbits pretreated with the staphylococcal superantigen toxic shock syndrome toxin 1, *Infect. Immun.*, 2001, **69**(11), 7169–7172.

54 A. Mobed and M. Hasanzadeh, Environmental protection based on the nanobiosensing of bacterial lipopolysaccharides (LPSs): material and method overview, *RSC Adv.*, 2022, **12**(16), 9704–9724.

55 T. Ikeda, *et al.*, Comparative Evaluation of Endotoxin Activity Level and Various Biomarkers for Infection and Outcome of ICU-Admitted Patients, *Biomedicines*, 2019, **7**(3), 47.

56 J. Chung, *et al.*, Effects of storage conditions on the performance of an electrochemical aptamer-based sensor, *Sens. Diagn.*, 2024, **3**(6), 1044–1050.

57 S. Arshavsky-Graham, *et al.*, Aptamers *vs.* antibodies as capture probes in optical porous silicon biosensors, *Analyst*, 2020, **145**(14), 4991–5003.

58 R. M. Mayall, *et al.*, Ultrasensitive and Label-Free Detection of the Measles Virus Using an N-Heterocyclic Carbene-Based Electrochemical Biosensor, *ACS Sens.*, 2020, **5**(9), 2747–2752.

59 U. Ohto, *et al.*, Toll-like Receptor 9 Contains Two DNA Binding Sites that Function Cooperatively to Promote Receptor Dimerization and Activation, *Immunity*, 2018, **48**(4), 649–658.e4.